Palacký University Olomouc
Faculty of Science

Department of Optics

Optical design and construction of a fluorescence microscope for single-photon emitter imaging

Master's Thesis

Anežka Dostálová

Palacký University Olomouc
Faculty of Science

Department of Optics

Optical design and construction of a fluorescence microscope for single-photon emitter imaging

Master's Thesis

Author:	Bc. Anežka Dostálová
Study programme:	N1701 Physics
Field of study:	Optics and Optoelectronics
Form of study:	Full-time
Supervisor:	RNDr. Miroslav Ježek, Ph.D.
Co-supervisor:	Mgr. Robert Stárek, Ph.D.

Thesis submitted on: 28 April 2023

Univerzita Palackého
Přírodovědecká fakulta

Katedra optiky

Realizace optické části fluorescenčního mikroskopu pro zobrazování jednofotonových emitorů

Diplomová práce

Autor: Bc. Anežka Dostálová
Studijní program: N1701 Fyzika
Studijní obor: Optika a optoelektronika
Forma studia: Prezenční
Vedoucí: RNDr. Miroslav Ježek, Ph.D.
Konzultant: Mgr. Robert Stárek, Ph.D.

Práce odevzdána dne: 28. dubna 2023

Abstract

The aim of the thesis is to design and build a fluorescence microscope for imaging single emitters and examining the properties of the emitted non-classical light. Fluorescence microscopy is a powerful imaging technique that utilizes fluorophores to visualize biological samples and processes. Fluorophores are molecules capable of fluorescence, and since a single molecule can only emit one photon at a time, the detected signal is inherently non-classical. The steps taken in this thesis to achieve light of single-photon nature include the mechanical and optical design of the microscope setup, preparation of a suitable sample of terrylene molecules embedded in a para-terphenyl crystal and analysis of the fluorescent light. Most importantly, the second-order correlation function at a zero time delay was measured by means of the Hanbury-Brown and Twiss experiment. A value of $g^{(2)}(0) = 0.25$ was obtained, which is a clear characteristic of non-classical antibunched light.

Keywords

`Fluorescence microscope, single-molecule fluorescence, terrylene, p-terphenyl, spin coating, TIRF, Hanbury-Brown and Twiss, second-order correlation function, photon antibunching, single-photon source`

Acknowledgments

First and foremost, I would like to express deep and sincere gratitude to my supervisor RNDr. Miroslav Ježek, Ph.D. for providing me with invaluable guidance, advice, encouragement and overall support, as well as for all his work in general. His expertise, insights and enthusiasm have been a key element for my motivation and endeavour. I would like to extend my sincere appreciation to my co-supervisor Mgr. Robert Stárek, Ph.D. for his priceless advice and guidance especially in the lab, for sharing his remarkable knowledge with me and for relevant feedback. I also wish to convey my thanks to everyone in the Department of Optics for making the research possible and for creating a friendly and inspiring working environment, and to all the lectors for their helpfulness and time they devoted to us not only during the lectures. I am grateful to my colleagues and friends together with whom we shared the years of studies, overcame all the obstacles and experienced a great amount of joy. Special thanks go to Daniela, Dominik and Filip, whose support is beyond words. I would also like to thank my life-long friends who are now in various fields of study and share their life experiences with me, as well as friends from all over the world who entered my life during my master's studies and have been a valuable inspiration to me, and my boyfriend for his love and encouragement. Finally, I want to express my deep thanks to my family for their unwavering support, patience and invaluable help throughout my whole life.

Anežka Dostálová

Declaration

I hereby declare that I have written this Master's Thesis—and performed all the presented research and experimental tasks—by myself, while being supervised by RNDr. Miroslav Ježek, Ph.D. I also state that every resource used is properly cited. I agree with the Thesis being used for teaching purposes and being made available at the website of the Department of Optics.

Signed in Olomouc on ....

Anežka Dostálová

Contents

Chapter 1

Introduction

Quantum optics is a rapidly advancing field of physics that investigates the fundamental properties of light and its interaction with matter. Over the past decades, quantum technologies have been developed and grown in importance, such as quantum communication, computing, cryptography, and sensing. All these technologies are based on non-classical quantum states of light that are impossible to be obtained from classical light sources. Consequently, single-photon sources are of great importance, as they enable the emission of light in the form of single photons leading to the generation of the target states with non-classical properties.

Various approaches have been devised to attain single-photon sources. One of the methods is based on spontaneous parametric down-conversion, a nonlinear process producing photon pairs, which was suggested for the non-classical light generation [1] and has been widely used since [2]. However, such sources are probabilistic. Another possibility is the usage of a system that has to be re-excited before it can emit a new photon, for instance a single atom, ion, colour centre, quantum dot, or a single molecule [3]. All of these systems have been investigated in quantum optics experiments and protocols. Single atoms were used as single-photon sources in works [4, 5], and single ions were proposed for this purpose [6]. Single photons produced by an excitation of nitrogen-vacancy (NV) colour centre in diamond were used [7] and the authors of [8] demonstrated a more efficient source composed of a nitrogen-vacancy centre in a diamond nanowire. An electrically driven single-photon source based on an NV centre at room temperature was realized [9]. Quantum dots have been utilized for single-photon generation [10, 11, 12], while [13] provides a recent review of the topic.

The single-photon source of primary concern in the context of this thesis is the single molecule. Absorption of a photon will excite the molecule to one of the vibrational states of the excited energy state S_1. After a non-radiative transition to the lowest vibrational state, the molecule can spontaneously relax back to the ground state S_0 by emitting a photon of lower energy than that of the incident photon. Only one photon at a time can be emitted via the $S_1 \rightarrow S_0$ transition, and new excitation is necessary before another photon emission can occur. The emitted light is therefore antibunched, which was first observed for molecules in works [14, 15], and is referred to as fluorescence. A source of single photons on demand at room temperature was presented [16], and an overview of the underlying principles is given in [17]. More recent publication [18] demonstrates a very regular

stream of single photons emitted by a single molecule. The molecule-based single-photon sources may even be tunable, as was achieved in [19] by applying uniaxial strain fields.

In practice, the molecules are always embedded in a host material. A wide range of molecule–host combinations has been explored at cryogenic and room temperatures. Typical fluorophores, i.e. molecules capable of fluorescence, are terrylene, perylene, pentacene, and rhodamine. Hosts can vary in their phase; both liquid and solid hosts have been studied and are commonly used. The choice of a host material depends on the specific experimental requirements and application. Single fluorescent molecules can be dispersed in liquid media such as solvents, polymer matrices, or lipid membranes. These hosts provide a highly dynamic environment, which can be useful for studying molecular dynamics, chemical reactions, or biomolecular interactions. Solid hosts, on the other hand, provide a stable environment, the molecules are immobilized within a crystalline matrix and their position and orientation can potentially be precisely controlled. The solid hosts are a favourable choice in the case of studying properties such as the emission spectrum or fluorescence lifetime, and, most importantly, in the case of creating a single-photon source. A few specific examples of crystal hosts are p-terphenyl, n-hexadecane, and naphthalene. In recent years, interest in using hybrid hosts that combine the advantages of both liquid and solid hosts has been increasing to achieve optimal control over the molecular properties and environmental interactions. For instance, the authors of [20] used a liquid crystal host. In the experimental work presented in this thesis, we adopt a common combination of terrylene molecules embedded in p-terphenyl crystal.

Detection and localization of signals from single emitters have a wide range of applications in many research areas such as biophysics, biochemistry, and nanotechnology. Specialized imaging techniques are utilized for this purpose, including fluorescence microscopy and its subset called single-molecule localization microscopy (SMLM). These imaging techniques based on fluorescence allow for observation and tracking of individual molecules with high spatial and temporal resolution. Once the signals have been detected, the position of the emitter can be localized and the information can then be used for better understanding of fundamental processes at the molecular level. Furthermore, fluorescent labelling can be employed to extend the usage of these techniques beyond fluorophores, as these can be attached to other, non-fluorescent molecules of interest such as proteins, DNA, RNA and lipids, and enable their visualization in real time and the study of their structure and interactions as well. Another possible application of single emitters is quantum sensing [21] and the application of quantum metrology in biology is reviewed in [22].

Single-molecule localization microscopy enables precise localization of individual fluorescent molecules with nanometre-scale resolution computationally from diffraction-limited image sequences [23]. The acquired information is used to construct a superresolution image or the trajectory of the molecules. Other techniques such as interferometric scattering microscopy (iSCAT) enable the imaging of single nanoparticles or biomolecules [24]. The iSCAT microscopy is a label-free technique. The principle lies in detecting the interference of reference light and light scattered by the studied particle. In addition, it is also capable of determining the particle mass. Under ideal conditions, the limiting factor in iSCAT is the shot noise. In reality, however, other noise sources are present and consequently, the detection sensitivity might not be sufficient for molecules of arbitrarily low mass. The au-

thors of [25] utilized unsupervised machine learning for improvement of the mass sensitivity limit, representing just one example of growing importance of machine learning in single particle and emitter imaging.

The term superresolution was already mentioned in the previous paragraph and is yet another important example of the possible applications of single-photon emitters. In classical optics, the imaging resolution is restricted by the diffraction limit, there have nevertheless been efforts to surpass it. Quantum superresolution imaging method based on the non-classical fluorescent light is demonstrated in [26], supporting the claim that single emitters possess an extremely broad range of uses.

The goal of this thesis is to design and build a fluorescence microscope in order to enable further research in some of the listed applications of a single-photon source based on single organic molecules, such as superresolution, emitter localization and counting, or quantum sensing. The process of successful construction of the microscope includes preparation of the single-molecule sample and characterization of the emitted fluorescent light. Chapter 2 focuses on the single molecule system, introducing the theory of fluorescence emission. The particular choice of molecule–host combination of terrylene in p-terphenyl is specified and the sample preparation procedure described. Chapter 3 is dedicated to the fluorescence microscope. The mechanical design and selection of optical components are discussed and the building process and alignment of the whole setup is described in detail. The results of an analysis performed on the fluorescent signal emitted by the molecules are presented and discussed in Chapter 4. The final concluding chapter summarizes the work and states the future outlook and goals.

Chapter 2

Single molecule system

A specific kind of molecules, typically organic compounds, have fluorescence properties. This means that an incident photon of a certain wavelength can be absorbed by the molecule, causing its excitation to a higher energy level, and the molecule consequently emits another photon. The emitted photon has a lower energy, as will be explained later, and therefore has a longer wavelength. This process is known under the term fluorescence and the molecules capable of it are called fluorophores. Since a single molecule can never emit more than one photon at the same time, it becomes a good candidate for a single-photon source, which is the objective of this thesis. This chapter is dedicated to an explanation of the process of fluorescence in a single molecule, description of the particular choice of the molecule and the host, as well as sample preparation and characterization.

2.1 Single-molecule fluorescence

To describe the process of fluorescence from a single molecule, the molecule can be considered a two-level system. The two energy levels that play a role are the ground state S_0 and the first excited state S_1. The designation by the letter S comes from the fact that these states are singlet states, meaning that the electrons occupying them have anti-parallel spins and therefore their spin quantum number $S = 0$. The ground state is always a singlet state, the excited states on the other hand can have the spin quantum number S equal to both 0 and 1. The states with $S = 1$ have parallel spins, are known as triplets and typically have lower energy than the corresponding excited singlet state [27]. The terminology for singlet and triplet states originates in the multiplicity of energy levels defined as

$$2S + 1 = \begin{cases} 1 & \text{for } S = 0 \\ 3 & \text{for } S = 1. \end{cases}$$

The schematic visualisation of the molecular energy levels is shown in Fig. 2.1 in the form of a Jablonski diagram. Three possible states are depicted: the ground state S_0, the first excited singlet state S_1, and the first excited triplet state T_1. Each of the states has a finer structure of vibrational levels as the molecule also has vibrational energy. The process of fluorescence takes place between the singlet states S_0 and S_1. Upon interaction with light, the molecule can get into the first excited state through absorption of a photon of suitable energy. It can end up in

any of the vibrational levels and what follows is a non-radiative transition to the lowest vibrational level of the S_1 state. From there the molecule relaxes onto one of the vibrational levels of the ground state with the simultaneous emission of another photon. This photon emission is called fluorescence of the molecule. A molecule's lifetime is the average time between its excitation and return to the ground state.

It can be seen from the figure that due to the non-radiative transitions within both states, the emitted photon has a lower energy than the photon which was originally absorbed. This energy difference corresponds to a difference in wavelength $\Delta\lambda$ as these quantities are bound by the relation

$$E = h\nu = \frac{hc}{\lambda}, \tag{2.1}$$

where h is the Planck constant, c is the speed of light, and ν is the frequency of the photon. Since the energy of the emitted photon is lower, its wavelength is longer and the difference $\Delta\lambda$ is known as the Stokes shift.

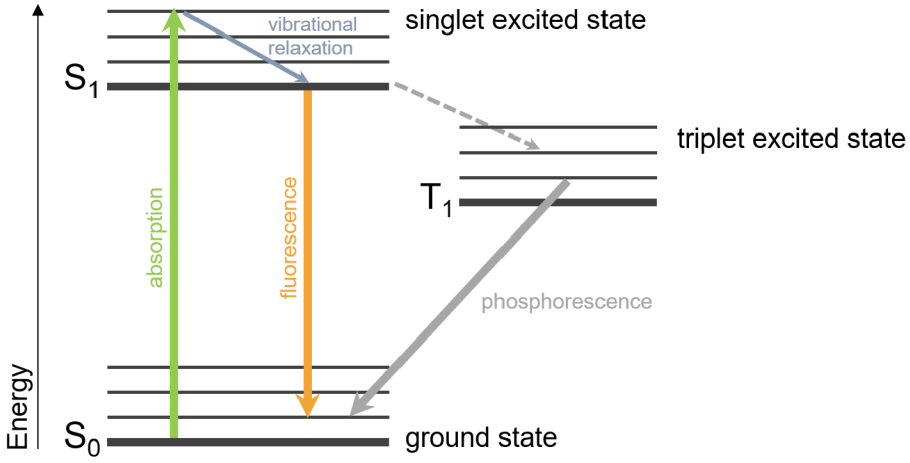

Figure 2.1: Jablonski diagram of single molecule energy levels. The ground state, singlet excited state, and triplet excited state are denoted S_0, S_1, and T_1, respectively. Each state is split into a fine structure of vibrational states. The process of photon absorption (green arrow) leaves the molecule in an excited state S_1. After a non-radiative transition (sand blue arrow) to the lowest vibrational state of S_1, the molecule can either emit another photon by fluorescence (orange arrow), or transit to the triplet state T_1 via a low-probability intersystem crossing and emit a photon by phosphorescence (grey arrow).

Absorption from the ground state to the triplet excited state is forbidden due to the fact that excitation by photons can only occur between states of the same spin [27]. There is, however, a non-zero probability of transition to the T_1 state from the S_1 state called intersystem crossing. The process $T_1 \rightarrow S_0$ takes place at much slower emission rate and is called phosphorescence. The probability of intersystem crossing for a single-photon emitter is nevertheless low enough for the triplet state to be neglected [17], only fluorescence processes will therefore be taken into account from now on.

2.2 Terrylene in p-terphenyl

The fluorescent molecules selected for our experiment are terrylene molecules. The choice is based on the availability of these molecules, their photostability and most importantly the ability of operation under room temperature conditions.

To be able to deposit the single molecules onto a coverslip to create a sample for observation under the fluorescence microscope, it is necessary to embed them in a host. Matrices such as polymers or glasses have been used at low-temperature conditions and the effects of spectral diffusion and blinking were observed which are almost absent in crystalline hosts [28] due to their well-ordered structure. Also, the fluorescence spectra of emitters embedded in polymers evolve with time, whereas the spectra of emitters in crystalline matrices have been shown to be stable [29]. A crystal host of p-terphenyl, which will be used in our experiment together with the molecules of terrylene, was first investigated at low temperature in works [30, 31]. The quality of the p-terphenyl sublimation crystals and the low concentration of the embedded fluorescent terrylene molecules enables one to observe the fluorescence at room temperature as well, as reported in [29]. Our experiment is performed entirely at room temperature, hence this combination of molecules and host is a suitable option.

Terrylene has the molecular formula of $C_{30}H_{16}$ and is a representative of conjugated hydrocarbons, i.e. organic compounds containing atoms of carbon and hydrogen with alternating single and multiple bonds between the carbon atoms. In particular, it belongs to a group of aromatic hydrocarbons which are characterized by a ring structure shown in Fig. 2.2. The formula of p-terphenyl is $C_6H_5C_6H_4C_6H_5$ and it also belongs to the group of aromatic hydrocarbons. It consists of three benzene rings. The molecular structure of both terrylene and p-terphenyl is shown in Fig. 2.3.

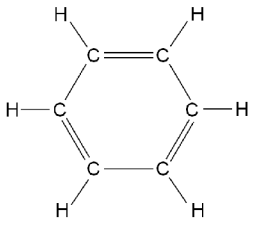

Figure 2.2: The basic unit of aromatic hydrocarbons, the benzene ring composed of hydrogen (H) and carbon (C) atoms with alternating single and double bonds.

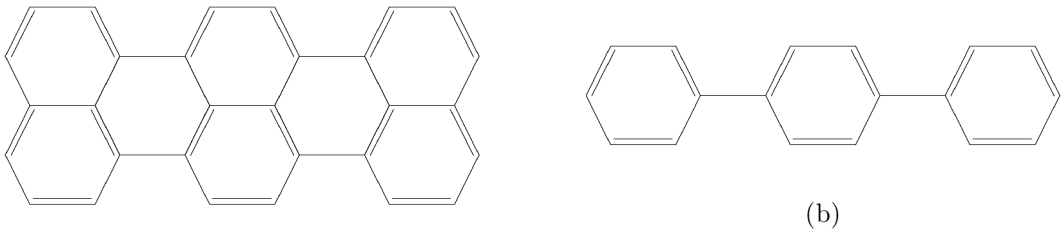

(a) (b)

Figure 2.3: The molecular structure of (a) terrylene and (b) p-terphenyl.

The crystalline organic host protects the fluorescent molecules from being exposed to diffusing quenchers, for example oxygen [16]. Consequently, the molecules exhibit good photostability, rapid bleaching is rare, and individual molecules which can endure long continuous illumination by excitation light can be rather easily found. The transition dipole moments of terrylene molecules are almost parallel to the optical axis, i.e. almost perpendicular to the sample plane. The orientation of the emitters is therefore well defined. It was shown in [32] that the emission from such oriented molecules has the form of a doughnut when imaged. An asymmetry of the shape is likely observed due to a small tilt of the dipole with respect to the optical axis [33].

2.3 Terrylene emission spectrum

Before any sample preparation, the first characterization of the terrylene was performed via the measurement of its spectrum. A plastic vial containing the solution of terrylene and toluene was fixed in a mechanical mount. An output of a laser with wavelength $\lambda = 532\,\mathrm{nm}$ was directed into the solution and strong yellow fluorescent signal was observed in all directions, see Fig. 2.4. With the use of a fiber collimator (Schäfter+Kirchhoff), a part of the fluorescence was coupled into a multimode optical fiber, which led the signal to a spectrometer (HR2000+, OceanOptics).

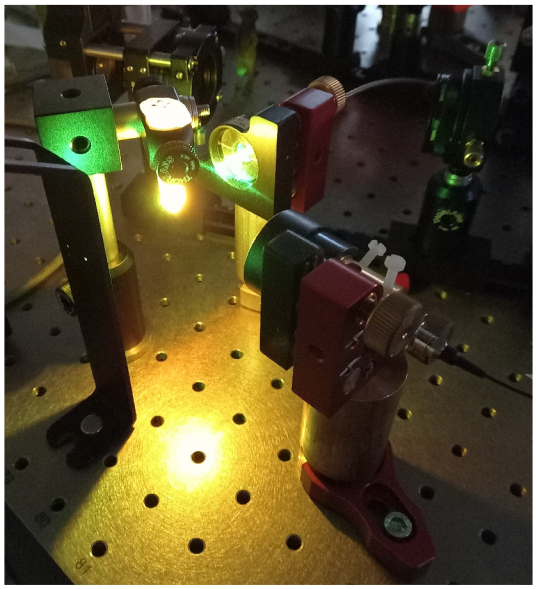

Figure 2.4: Fluorescent light emitted by a concentrated solution of terrylene molecules in toluene when excited by green laser light ($\lambda = 532\,\mathrm{nm}$).

The measured emission spectrum of terrylene can be seen in Fig. 2.5. It was obtained as an average of 30 acquired spectra, each with 1 s integration time. The central wavelength of the most significant peak is $\lambda = 579.7 \pm 0.2$ nm and was determined by fitting a Gaussian curve to data corresponding to the peak and finding the position of its maximum. Calibration of the spectrometer with the help of a calibration lamp (CAL-2000, Ocean Optics) was also taken into account. The uncertainty

of the wavelength determination is influenced by the spectrometer resolution and is considered to be its half. The second peak is centred at $\lambda = 616.0 \pm 0.2$ nm. A cut at the wavelength of $\lambda = 550$ nm can be seen, which is due to long-pass dielectric spectral filter (Semrock) used in order to filter out the intensive excitation laser light. The observed spectrum has a typical shape of a terrylene emission spectrum (see for example [29]).

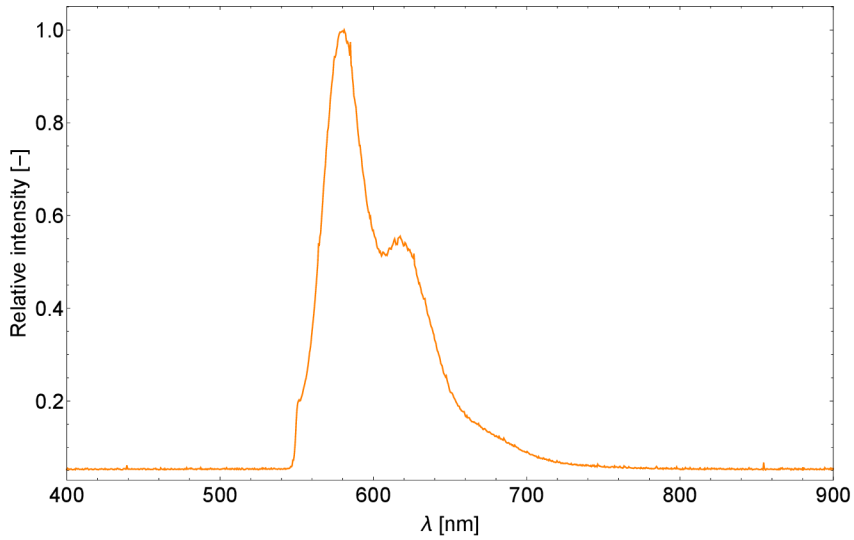

Figure 2.5: Measured spectrum of fluorescent light emitted by terrylene molecules in a concentrated solution.

2.4 Sample preparation

The samples utilized for observation and analysis of fluorescence signal in our microscope setup consist of p-terphenyl crystal host and terrylene molecules. The original procedure for doping the p-terphenyl with terrylene was cosublimation [29, 31] and the resulting sublimation flakes were glued on a substrate (LiF or glass). A new method, spin coating, for creating thin crystalline films of organic molecules was introduced in [34]. This technique was later applied to terrylene in p-terphenyl [33] and the authors showed that the fabricated thin film is of a crystalline nature with the terrylene molecules aligned perpendicular to the film plane. We adopt the approach of spin coating for preparation of our own samples.

Spin coating is a technique for depositing thin uniform films on flat surfaces. The spin coater device (L2001A3, Ossila) is shown in Fig. 2.6. It has a rotational plate with exchangeable chucks, designed to hold different substrate shapes in place, and a lid with a hole in the middle for applying the desired film material safely. The rotation speed and duration are fully programmable by the keypad. The material to be coated is applied to the substrate either while it is already rotating at certain speed or before any rotation takes place, depending on the particular procedure recipe.

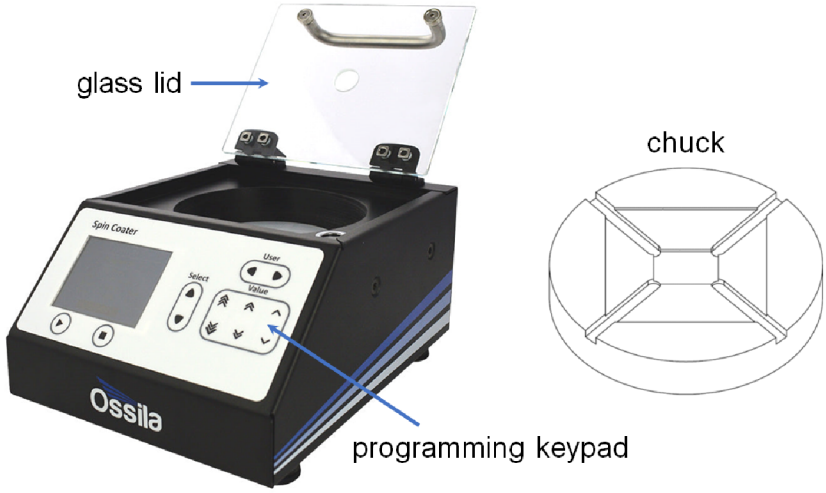

Figure 2.6: Commercial spin coater device from Ossila and an example of a chuck for the substrate attachment. The illustrations without the labels come from the manufacturer's manual.

The chemical structure of both p-terphenyl and terrylene was already introduced. Both substances are in the form of a white (p-terphenyl) and black (terrylene) powder and, as the first step in the process of sample preparation by spin coating, they need to be diluted. The solvent is in both cases toluene. The procedure recipe adjusted for our purpose according to the amount of acquired ingredients is as follows:

- 500 mg of p-terphenyl is diluted in 75 ml of toluene.
- 10 mg of terrylene is diluted in 100 ml of toluene.
- The solution of terrylene and toluene is further diluted in toluene in a ratio of 1:10 ml.
- 20 µl of the diluted solution of terrylene and toluene is mixed with 75 ml of the solution of p-terphenyl and toluene.

The final solution is then applied with a pipette onto a glass coverslip fixed in a suitable chuck in the spin coater. The coverslip must be properly cleaned beforehand with appropriate chemicals. First it was sank inside of a beaker filled with acetone and placed into an ultrasonic bath for 10 minutes. The same procedure was repeated with propanol.

The maximum volume that can be spin coated is 20 µl. The samples created according to the recipe above have rather a high concentration of terrylene molecules. It is therefore useful for the first tests and trials of the microscope setup, because the fluorescence signal comes from a large number of molecules simultaneously and can be easily seen and used for alignment of the emission path (see Sec. 3.5). For single-photon experiments, however, the concentration of emitters must be low, and to achieve this, the following steps are added to the recipe:

- The solution of terrylene in toluene is diluted once again by mixing 20 µl of the previous solution with 10 ml of pure toluene.
- 250 mg of the host p-terphenyl is diluted in 38 ml of toluene and 20 µl of the solution from previous point is added to produce the final substance.

The resulting concentration of the dopant molecules in the host is $c = 7.4 \times 10^{-9}$. The spin coating procedure is the same as in the previous case. The device is programmed such that it rotates with the speed of 1500 RPM (revolutions per minute) for 30 s and then it accelerates up to 3000 RPM for 3 s, which is supposed to ensure that all possible redundant liquid is gone after the procedure is completed. The result is a thin crystalline film of p-terphenyl doped with terrylene molecules deposited on a glass coverslip, which is used as a sample in the fluorescence microscope described in the following chapter. Examples of the terrylene-doped crystals can be seen in Figs. 2.7 and 2.8.

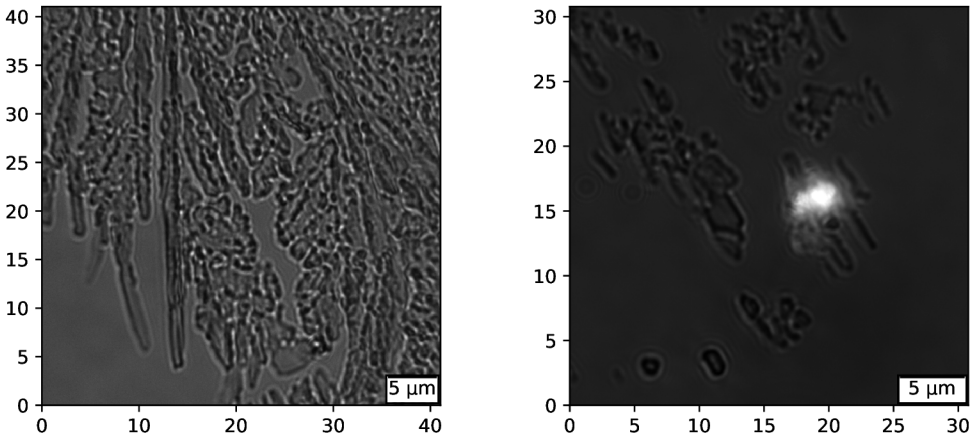

(a) (b)

Figure 2.7: (a) An example of a p-terphenyl crystal deposited on a coverslip via spin coating, imaged by the microscope setup with the use of an auxiliary LED illumination. (b) An image of a p-terphenyl crystal under the laser excitation illumination by a focused beam. Strong fluorescence emitted by terrylene molecules in the illuminated area is observed. The emission is strong and clearly visible due to the fact that the sample contains a high concentration of terrylene molecules and a large number of them is excited at the same time.

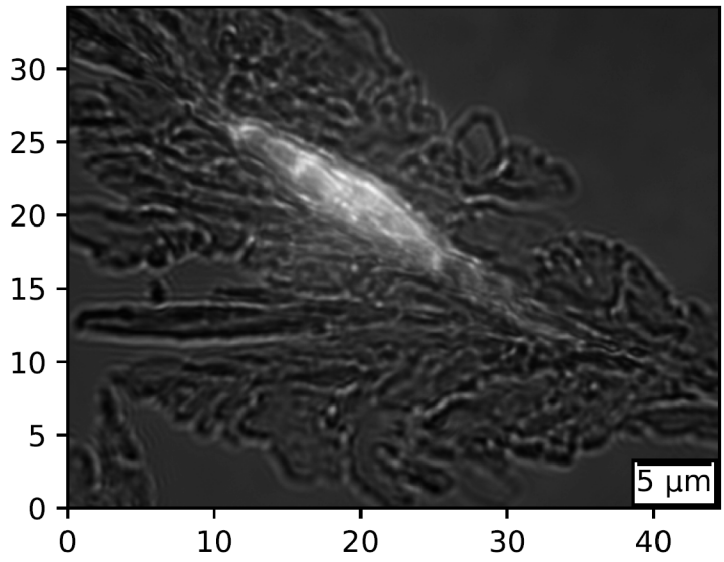

Figure 2.8: A camera image of a p-terphenyl crystal doped with terrylene molecules under wide-field illumination by the excitation light, achieved by adding an extra lens into the setup so that molecules in a larger area of the sample are excited (details of the purpose of each optical component will be discussed in the following chapter).

Chapter 3

Fluorescence microscope

Fluorescence microscopy is a technique which uses fluorescent light to obtain unique characterization of the sample on the level of single molecules. The general principle lies in an illumination of a sample by an excitation laser beam and a collection of light emitted by the excited molecules in the sample. The sample typically contains fluorescent molecules embedded in an appropriate host material. A fluorescent dye, fluorescent chemical compound, may also be used for labelling non-fluorescent biomolecules such as proteins, allowing to track them or study their properties individually within the sample. Fluorescence microscopy has therefore become an essential tool in various fields of biology, including cell biology, microbiology, and neuroscience. From quantum optics point of view, fluorescence microscopy can be considered a feasible way of realizing a single-photon source and provide insights into the fundamentals of quantum systems, their interaction with the environment and dynamics under different experimental conditions, all of which is invaluable for quantum information processing or communication.

3.1 Principle of operation

The setup of a fluorescence microscope is generally composed of two fundamental parts, an excitation path and an emission path. The purpose of the excitation path is to illuminate the sample and cause it to emit photons of lower energy, i.e. longer wavelength, by the process explained in Sec. 2.1. The emitted light is collected in the emission path which is concluded by detection. The two paths overlap in the vicinity of the sample and the crucial step is to separate them. This is achieved by a dichroic mirror, an optical component with different reflection and transmission properties for different wavelengths. Typically, the excitation light of shorter wavelength is reflected in the direction of the sample, whereas the longer-wavelength emitted light is transmitted towards detection, as illustrated in a simplified scheme in Fig. 3.1.

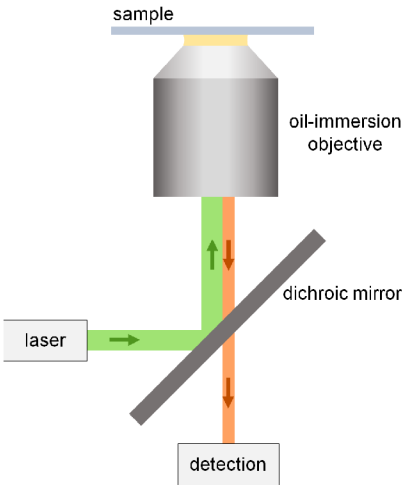

Figure 3.1: A simple scheme of the fluorescence microscope core. The excitation light illuminates the sample through an oil-immersion objective and the emitted fluorescence light is separated by a dichroic mirror.

3.2 Design

The design of the fluorescence microscope built in our lab was guided by the basic principles of operation described above. The main challenge concerned the choice of appropriate components and the sample attachment and illumination through an objective. The solution turned out to be a tall stage with the sample placed on top and illuminated through the objective from below. The stage is consistent of four robust pillars screwed directly into the optical table, two custom metal plates supporting the objective mount as well as a piezo stage (P-545.3C8S, PInano) onto which a sample holder is attached, and three balls allowing the movement of the upper plate to be as smooth as possible. A 3D model of the stage created in Autodesk Inventor can be seen in Fig. 3.2.

The piezo stage is necessary for a precise controlled movement of the sample holder allowing scanning through the sample. In order to have the option of a coarse scanning, the upper plate is also placed on two manual linear translation stages in x and y directions. The objective is mounted on another linear stage enabling the first iteration of focusing before employing the precise piezo stage.

The process of building the experimental setup involved designing several custom parts. The metal frames for the microscope stage were already mentioned, another example is the sample holder, a thin metal plate screwed directly into the piezo stage by M2 screws. The coverslip with the sample is then attached by tiny magnets.

Custom holders for two collimators with long focal lengths (35 mm and 40 mm) providing large-diameter beams were also necessary. The collimators were acquired specifically for our setup and thus no suitable mounts were available in our lab. The lens position within the collimator with respect to the optical fiber end-face must be adjusted properly by an eccentric key in order to obtain a collimated beam at the output. The hole for the eccentric key therefore has to be accessible through the mount, as well as the clamp screw for locking the final lens position. The location

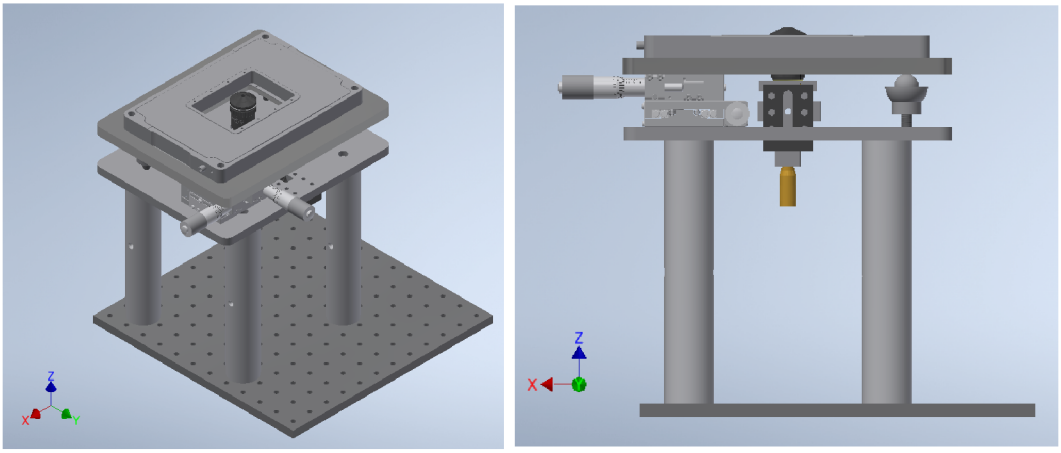

Figure 3.2: 3D model of the microscope stage, the core of the whole setup where illumination of the sample takes place and the excitation and emission paths overlap. Linear stages and a precise piezo stage allow controlled movement of the sample in all x, y and z axes.

of holes in the holder to maintain this access was calculated based on a drawing of the collimator provided by the manufacturer. Fig. 3.3 shows the created drawing of the 35 mm collimator holder and the fabricated result made of brass.

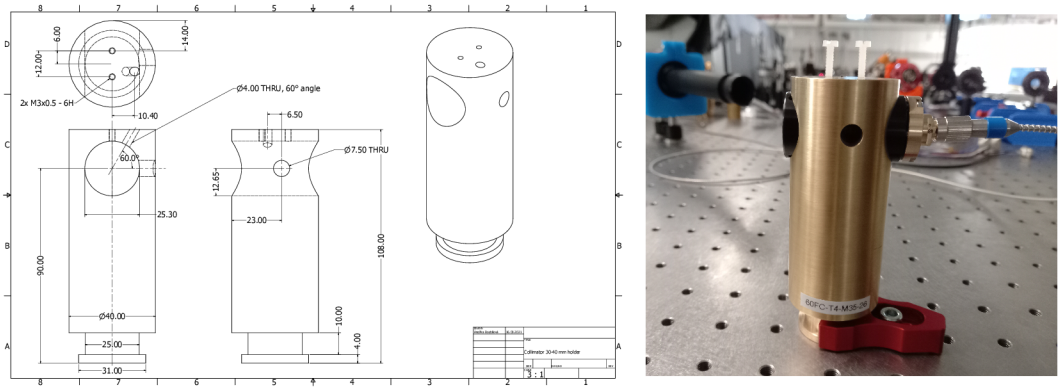

Figure 3.3: Drawing of the custom holder for a 35 mm collimator and the fabricated product.

The experimental setup of the microscope constructed in our lab is shown in Fig. 3.4. The excitation path starts with a continuous laser with a polarization-maintaining (PM) single-mode optical fiber. The signal is out-coupled into free space by a collimator and two mirrors are used to properly set the height and path of the beam. Power and polarization control components such as a neutral density filter (ND) and half wave plate (HWP) are used. Two other mirrors follow to guide the beam around the microscope stage and a lens in a flip-mount is placed between them with the aim of having the option to switch to a wide-field illumination. In the default, the lens is not a part of the setup and the sample is illuminated by a focused excitation beam. It is nonetheless sometimes convenient to illuminate a larger area of the sample simultaneously and it is for this purpose that the lens

can be added. It is placed in the distance of one focal length in front of the back focal plane of the objective such that the beam emanating from the objective is collimated. After the optional wide-field lens, the excitation laser beam is directed by the second mirror to the crucial component, the dichroic mirror (DM), which reflects it towards the stage. A mirror in a 45° mount reflects the beam upwards into the objective to illuminate the sample placed on the piezo stage. Fluorescence signal (orange) is emitted by excited molecules in the sample, travels back through the objective and is transmitted by the dichroic mirror into the detection block. The detection can be performed by a camera, a spectrometer, or a combination of single-photon detectors and a beam-splitter as will be discussed in Sec. 3.5, depending on the desired analysis of the fluorescence signal.

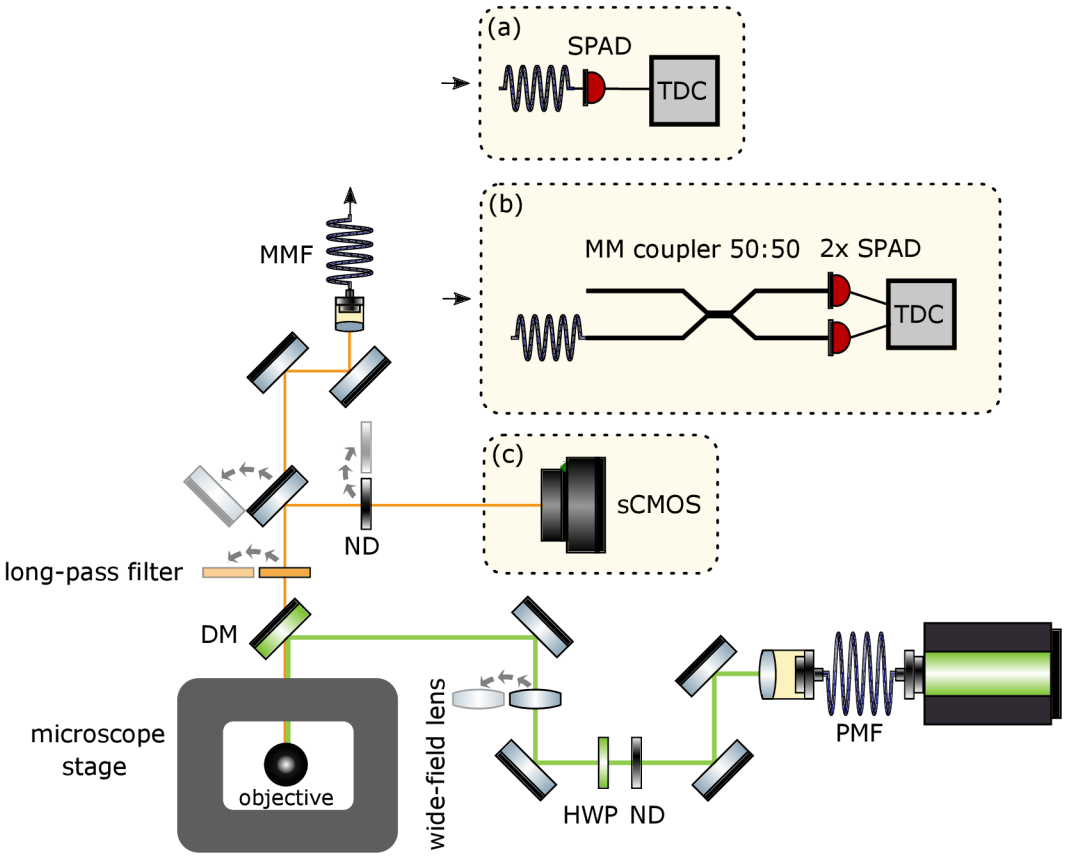

Figure 3.4: Experimental setup of a fluorescence microscope. The purpose of the excitation path (green) is to illuminate the sample and excite individual molecules, which in turn emit fluorescence light (orange) of different wavelength. The fluorescence is separated from the excitation at the dichroic mirror and different kinds of analysis can be performed on the signal with the right choice of detection scheme. (a) A simple single-photon detection with the use of a SPAD and a time tagger. (b) Hanbury-Brown and Twiss setup for coincidence measurement. (c) A sCMOS camera detection for classical imaging.

3.3 Optical components

Before the setup shown in Fig. 3.4 could have been built, appropriate optical components with the required properties had to be selected and acquired. This section describes each component in more detail and gives justification for the particular choices.

Laser The excitation beam is provided by a continuous laser (MatchBox, Integrated Optics) with wavelength $\lambda = 532\,\text{nm}$ and a spectral width $<0.025\,\text{nm}$ as reported by the manufacturer. It is of a very compact size and equipped with a Peltier cooler for thermal stabilization. The output optical fiber of our choice is a polarization-maintaining (PM) fiber with an APC connector (angled physical contact, where the fiber ferrule is polished at an angle) in order to minimize back reflections.

Collimator The collimator is an optical component for out-coupling light from an optical fiber into free space which is capable of producing a collimated beam, i.e. a beam of constant diameter over a long distance. It can also be used in reverse for coupling a signal into the optical fiber. The first collimator in our setup follows right after the PM fiber of the laser. It was chosen such that the out-coming beam has a large diameter, but is not cut by any of the other optical components, which might be an issue especially in the case of mirrors which are always placed under 45° angle with respect to the optical axis and their effective aperture is thus smaller by a factor of $\sin(45°)$. The chosen collimator is the 60FC-T-4-M35-26 from Schäfter+Kirchhoff with a focal length of $f = 35\,\text{mm}$. Its fiber connector is of the APC type. The collimator itself consists of an achromat with anti-reflective coating in the range of $420-700\,\text{nm}$.

Mirrors All mirrors in the setup are broadband dielectric mirrors BB1-02 from Thorlabs with 1 inch diameter made out of fused silica. 02 means that their coating is in the range of $400-750\,\text{nm}$, which covers both the excitation and emission wavelengths in our setup.

Neutral density filters In order to have control over the laser power, six neutral density (ND) filters with different optical densities (OD) were placed into a filter wheel, which is a convenient mount allowing the change of filters simply by its rotation. The optical density specifies the attenuation of the incident beam caused by the filter and is in direct relation with the transmission $T = 10^{-\text{OD}}$. The used ND filters are from Thorlabs and have OD = 0.5, 1, 2, 3, 4, 5.

Wide-field lens The wide-field lens is a lens that can be optionally added into the setup by means of a flip-mount and its purpose is to produce a collimated beam after the objective, which in turn results in illumination of a larger sample area. For this to work, the lens must be placed one focal length in front of the objective back focal plane. Taking into consideration all the components which must be inserted between the lens and the objective, the focal length of the lens needs to be long enough to provide sufficient space. A lens with $f = 500$ mm was therefore chosen,

specifically an achromatic doublet with coating in the proper wavelength region, AC254-500-A-ML from Thorlabs.

Dichroic mirror The dichroic mirror (DM) is a crucial component of the setup as it separates the desired fluorescence signal from the excitation laser light. It therefore has to have the right coating so that it reflects the wavelength 532 nm of the laser and transmits the fluorescence light of 580 nm. DM which was found to fulfil all the requirements is a component FF538-FDi02-t3-25x36 from Semrock. It has a single edge at 538 nm, reflecting shorter wavelengths and transmitting longer ones as desired. It has a shape of a 25×36 mm rectangle, therefore a special mount from Liop-Tec had to be purchased as well.

Objective An equally important component at the heart of the microscope is the objective. Typical microscope objectives are composed of several lenses and have very short focal lengths. In the case of our setup, high numerical aperture (NA) is particularly important. NA characterizes the ability of the objective to collect light in terms of the angle range, $\mathrm{NA} = n \sin(\theta)$, where n is the refractive index of the medium between the objective lens and the sample. It is therefore possible to increase the NA by increasing the medium refractive index, which is best achieved by filling the space between the objective and the sample with immersion oil whose refractive index is close to that of the glass coverslip. The objective engaged in our setup is UPLSAPO100XO from Olympus with 100× magnification and NA = 1.4 and is used together with IMMOIL-F30CC immersion oil.

Long-pass filter Even though the dichroic mirror is designed such that it reflects the 532 nm laser light, its reflectance is not perfectly 100 % and a small percentage of the excitation light will be transmitted into the emission path, which will be quite significant considering the typical laser power in comparison with the weak fluorescent signal. This can be used for alignment purposes as it allows observation of the laser spot on the camera. However, in most cases only the fluorescence emitted by excited molecules is of interest, and the laser light becomes parasitic and has to be eliminated. A properly chosen long-pass filter will assure exactly that. A Thorlabs filter FEL0550 with a cut-on wavelength 550 nm was therefore mounted in a flip-mount so that its presence in the setup is optional and the flexibility of signals entering the detection part kept.

Camera An sCMOS camera is used as one option of detection, especially in the building process and adjustment of the setup, but also later for classical imaging of the sample. The particular choice to start with was the camera ZWO ASI1600 with pixel size of 3.8 µm, quantum efficiency peak value QE = 60 % and the minimum read noise of 1.2 e^-. The camera was recently upgraded to Andor Marana 4.2B-6 with pixel size of 6.5 µm and QE up to 95 % in the region of wavelengths of our interest.

Optical fiber for fluorescence coupling Analysis of the emitted fluorescence light is of high interest and hence relevant devices will be used, many of which require an optical fiber input. It is thus necessary to couple the signal into an optical fiber

GIF625 (graded-index fiber with 62.5 µm core diameter), which is a multimode fiber as it is vital to couple as much of the signal as possible.

Fiber beam splitter Two single-photon detectors are needed for a coincidence measurement and photon antibunching verification, the fluorescence signal thus has to be divided into two branches travelling towards both detectors with the use of a fiber beam splitter. Since there are two detectors, two outputs are required, and consistently with the first fiber, the fibers of the BS should also be multimode. A suitable choice is the 2×2 multimode fiber beam splitter FOC F501278.

Single-photon detectors Single-photon detectors are necessary for analysis of the fluorescence signal emitted by single molecules. The detectors used in our experiment are single photon avalanche diodes SPCM-AQRH-14-FC, PerkinElmer/Excelitas, which are capable of detecting single photons in the range of wavelengths $400-1060$ nm. They are based on temperature controlled silicon avalanche photodiodes operated in Geiger mode and actively quenched. The maximum dark count is 100 Hz and the maximum dead time 65 ns, with the measured values even lower.

3.4 Excitation path

Once all the necessary components were available, construction of the setup could begin with the excitation path. The first step was to out-couple the laser light from the PM single-mode fiber into free space with the use of the 35 mm collimator. To ensure a collimated beam over a large distance, the optical path was prolonged to several metres with the help of three mirrors and the beam width was measured at various points with a beam profiler. The same beam width over the whole range was achieved by adjustment of the collimator lens position with an eccentric key. To achieve better precision, the collimation was later performed with the use of a shear plate and Shack-Hartmann wavefront sensor.

Since the custom collimator holder is fixed, two mirrors in tip-tilt mounts were added into the path so that the beam height and direction can be precisely set and controlled. To align the beam properly in the constant height of 90 mm above the optical table and straight above a line of thread holes, two irises were used, the second one as far in the desired direction as possible. The iris mounts were screwed directly into the thread holes of the optical table to make sure their centre is precisely positioned. A power meter (PM100D, Thorlabs) was placed after the second iris. Each mirror mount has two adjustment screws for tip and tilt and these are employed in a walk-in method of beam alignment. One of the adjustment screws is moved to one side and a maximum power reaching the power meter is found by adjusting the corresponding screw on the second mount. The same step is performed for the other pair of screws and the whole process is repeated iteratively several times until the maximum power is obtained.

These steps led to a well-aligned collimated excitation beam at the input of the fluorescence microscope setup. Some space was left for additional components like neutral density filters or half-wave plate for power and polarization control and two more mirrors followed to enable full control over the beam impinging on the subsequent crucial component, the dichroic mirror (DM). The same alignment

procedure for a straight beam of constant height as before was performed with the new pair of mirrors. The rectangular mount holding the DM was placed on a linear stage so that it can be accurately shifted back and forth in the direction of the excitation beam propagation for two reasons, the first one being an easier adjustment of the reflected beam position. The second and main reason is a transition between two regimes of fluorescence microscopy – normal incidence and TIRF – by means of shifting the DM. Both regimes will be discussed in more detail in Sec. 3.6. The angle of the DM was set to 45° with respect to the beam propagation with the help of two irises screwed into the relevant line of optical table thread holes.

The beam reflected by the DM needs to be navigated into the objective, which is vertically fixed in the microscope stage as seen in Fig. 3.2. A mirror in a 45° mount (H45, Thorlabs) is thus placed in the middle of the space between the pillars on an additional linear stage for an easier and more precise adjustment of the centre position. It is essential that the beam reflected upwards is perfectly straight and perpendicular to the optical table as it has to pass through the centre of the objective before illuminating the sample. The beam is therefore aligned in the absence of both the objective and the sample at first. Instead, two irises are mounted vertically in the objective mount with the help of extension tubes and a power meter sensor is seated at the top. A walk-in alignment method is employed again, using the adjustment screws on the dichroic mirror and the 45° mirror. To verify that the beam is hitting the sample under normal incidence, a microscope slide was placed in a custom-made holder and the back reflection was observed. In the case of normal incidence, it naturally has to follow the same path as the incident beam.

The crucial imaging component, the objective, is mounted into the stage once the straight vertical beam is ensured. Since it is an oil-immersion objective, a drop of an appropriate immersion oil has to be applied to the lens before a sample is attached. The oil then connects the objective and the bottom side of the coverslip with a sample on the top. The beam exiting the objective is focused on the sample plane.

It was already mentioned in the list of optical components that an additional lens can be added into the existing setup in order to generate a collimated beam behind the objective rather than a focused one. The obtained advantage is an illumination of a larger sample area and thus an easier scanning of the sample. However, this feature needs to be optional and it has to be possible to switch between these two modes readily, the wide-field lens is therefore placed in a flip mount. For the beam exiting the objective to be collimated, the lens must be located in a distance of one focal length ($f = 500$ mm) from the objective back focal plane.

The space between the two mirror pairs in the beginning of the path is used for components allowing control over the laser power entering the microscope, namely ND filters and a HWP. A wheel mount containing ND filters with different optical densities gives the opportunity to switch between power values by the order of magnitude. For finer adjustment, the software control of the laser pump current can be used.

An auxiliary white LED source is fixed in a mount just above the sample to enable the usage of the microscope setup for classical imaging, in order to see the structure of the crystal or any other potential sample, and for adjustment.

3.5 Emission path and detection

In case the sample contains terrylene molecules as described in Sec. 2.4, they can be excited by the laser light and emit fluorescence signal with the measured peak wavelength $\lambda = 579.7 \pm 0.2$ nm. The path this signal propagates along is then called the emission path. It therefore begins in the sample plane with a divergent beam a part of which is collimated by the objective. The fluorescence light is then reflected by the 45° mirror under the objective towards the dichroic mirror, where the essential separation from the excitation light takes place due to the emitted light being transmitted rather than reflected.

What directly follows the DM is a long-pass filter in a flip mount. Most often its effect of filtering out the portion of laser light that managed to leak through the DM is desired, but in some situations, it can become useful to observe the laser spot on the camera and then the filter can be removed temporarily. Since the excitation path was already well aligned and the first part of the emission path is identical, it is also well aligned to start with.

The next component is another type of flip mount containing an ordinary mirror whose purpose is to direct the signal into a detection type of choice. It can either be captured by a camera or by a more complicated detection setup. Since the camera imaging is used mostly for stronger signals and alignment purposes, it is not a significant problem if another few percent of the power are lost on the mirror in contrast with the more sophisticated detection methods where all the signal possible is needed. The flip mount also has a certain repeatability error which would cause a serious complication in the case of incoupling the signal into a fiber as it is very sensitive and a new adjustment would be needed every time the mirror is flipped, whereas it is not an issue if the image on the camera is shifted by a few pixels. The camera is therefore placed at 90° angle with respect to the direction of propagation so that the mirror is an active part of the setup in order to reflect the light towards it. The position and angle of the mirror are aligned such that the observed field of view is symmetric. An additional ND filter is inserted in a flip mount right in front of the camera and is used when the leaked laser light is present so that the camera chip is not overexposed. A tube lens ($f' = 200$ mm) is used to relay the image onto the camera chip. Before the camera was used for imaging in the lab, the tube lens was focused on "infinity" by pointing the camera out of the window and focusing on a distant object. By the objective design, the ideal corresponding tube lens would have the focal length of $f'_{\text{ideal}} = 180$ mm, the overall magnification is therefore scaled by the ratio f'/f'_{ideal}, yielding

$$M = M_{\text{obj}} \cdot \frac{f'}{f'_{\text{ideal}}} = 100 \cdot \frac{200}{180} \approx 111. \tag{3.1}$$

If the camera mirror is flipped away, the fluorescence light propagates straight forward and is coupled into a multimode fiber (MMF) with the help of two mirrors in tip-tilt mounts and a fiber collimator 60FC-0-A11-01 (Schäfter+Kirchhoff). The in-coupling of such a weak signal is a demanding process. Therefore, we exploit the laser light leaking through the dichroic mirror as its path overlaps with that of the fluorescence light. The input power can be increased for this purpose to increase

the leaked portion as well and make it even easier to work with. The process of in-coupling started with aligning the height and direction of the beam by a walk-in method using the mirror pair and two irises. When a properly aligned beam was obtained, the irises were replaced by the fiber collimator. Its position was slightly adapted by the screws of its own mount until the light was going through. The next step was to connect a fiber (GIF625) into the collimator and attach the other end to a power meter, followed by another iteration of the walk-in alignment method to obtain the maximum power behind the fiber.

With the fluorescence light coupled into a fiber, different kinds of analysis can be employed by connecting the fiber into different devices. The first one to mention is an optical spectrometer (HR2000+, Ocean Optics) which together with a software (OceanView) provides the spectrum of the signal. Other information can be obtained by employing a single photon detector such as a single photon avalanche diode (SPAD). The fiber is inserted directly into the SPAD, which is connected to a time-to-digital converter (TDC). The number of registered counts can then be observed on the computer. Since the SPAD is extremely sensitive, the influence of other light sources has to be eliminated. All lights where possible should be turned off and the detector, fiber and collimator covered with a black cloth. Extra shielding can be attained by a black hardboard built around and over the detection block.

Further expansion of the detection scheme lies in adding a second SPAD of the same type with the goal of measuring coincidences between photon detection from both detectors. To engage both SPADs, the fluorescence signal needs to be divided by means of a 2×2 fiber beam splitter. One of its inputs is connected to the fiber into which the fluorescence light is coupled, the other input is left loose, covered with a cap. Both outputs of the splitter are inserted into the two SPADs, which are thereafter both connected to the TDC. This latest scheme for coincidence measurement is referred to as the Hanbury-Brown and Twiss experiment and detailed attention will be paid to this topic in Sec. 4.3.

3.6 Normal incidence and TIRF

Under the standard operation of a microscope, the excitation light propagates along the optical axis of the objective and illuminates the sample perpendicularly to the sample plane, i.e. under normal incidence. The laser light is focused by the objective in the absence of the wide-field lens and excites the sample in a region of size corresponding to the size of the focused spot. It is however not the only possible regime. The use of total internal reflection (TIR) gives rise to total internal reflection fluorescence (TIRF) microscopy. TIR can occur at the interface of two media with different refractive indices n_1, n_2 in case the light propagates from the medium with the higher refractive index ($n_1 > n_2$) and it means that all incident light is reflected back into the first medium rather than being refracted into the second one. Another condition for TIR to occur is that the angle under which the light is incident on the interface must be equal or higher than the critical angle θ_c

$$\theta_c = \arcsin\left(\frac{n_2}{n_1}\right). \tag{3.2}$$

When this condition is fulfilled in the case of sample illumination in fluorescence microscopy, all the excitation light is reflected at the coverslip–sample interface.

The situation is depicted in Fig. 3.5. An electromagnetic field in the form of an evanescent wave is generated on the side of the sample. The field is of the same frequency as the excitation laser light and its intensity decreases exponentially with distance from the interface. Efficient excitation of molecules therefore happens only in the vicinity of the interface (a few hundred nanometres at maximum) [35].
The exponential decrease is described by the equation

$$I_z = I_0 e^{-z/d}, \tag{3.3}$$

where I_z is the evanescent wave intensity at a distance z, I_0 is the initial intensity and d is the penetration depth of the evanescent wave [35]

$$d = \frac{\lambda}{4\pi} \left(n_2^2 \sin^2 \theta - n_1^2 \right)^{\frac{1}{2}} . \tag{3.4}$$

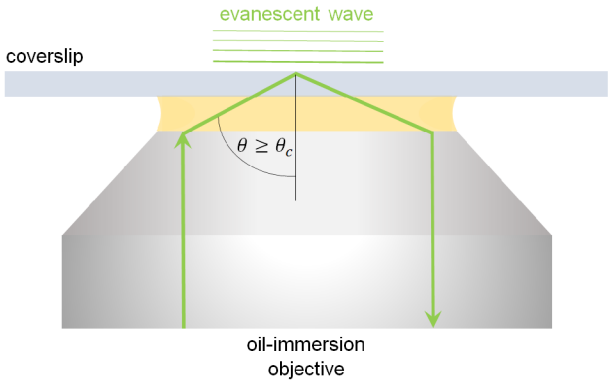

Figure 3.5: Total internal reflection fluorescence microscopy regime is achieved by illuminating the sample at a high angle. All the excitation light is reflected back into the objective and evanescent wave is generated at the coverslip–sample interface, exciting fluorescent molecules only in a thin layer of the sample.

The TIRF regime is achieved by introducing a shift of the excitation beam position in the back focal plane of the objective, i.e. a lateral shift of the excitation beam axis with respect to the objective optical axis such that they remain parallel. Experimentally it is accomplished by moving the dichroic mirror on a linear stage and consequently shifting the reflected beam. The main advantages of TIRF microscopy are better signal-to-noise ratio and elimination of out-of-focus fluorescent light.

Single terrylene molecules imaged in the TIRF microscopy regime appear on the camera in the shape of a doughnut, see Fig. 3.6. This is due to the molecules' transition dipole moments being oriented approximately perpendicularly to the sample plane, as discussed in Sec. 2.2, together with the fact that TIRF provides significant component of the excitation light electric field along these dipole moments [33].

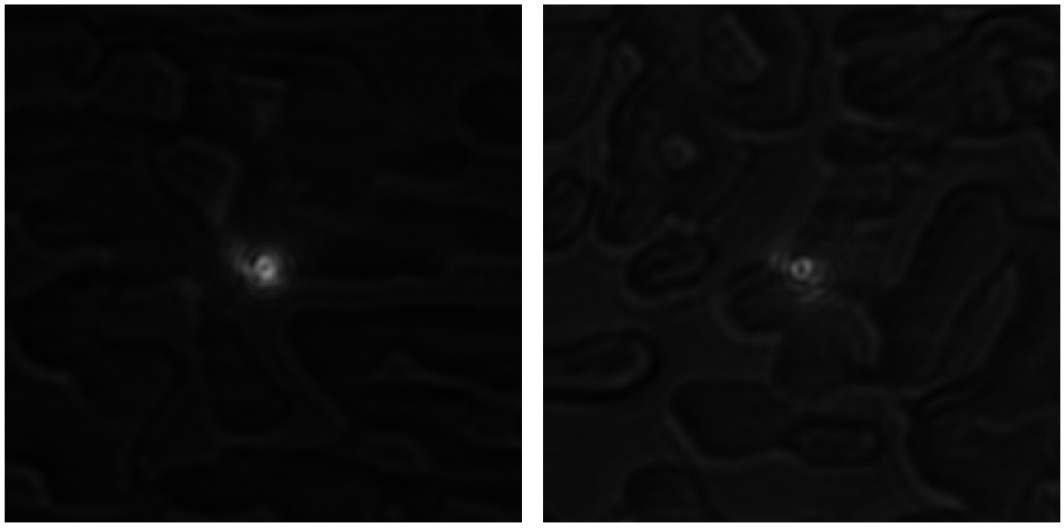

Figure 3.6: Doughnut-shaped single terrylene molecules captured by the camera in the TIRF microscopy regime.

Chapter 4

Fluorescence signal analysis

With a functioning fluorescence microscope setup, analysis of the fluorescence light emitted by excited molecules could be performed. Different detection possibilities were depicted in the setup scheme in Fig. 3.4. With the signal of interest coupled into an optical multimode fiber, however, any other suitable device can be easily connected and employed for gaining information. This chapter describes results obtained by several detection methods implemented for the characterization of the fluorescence signal emitted by terrylene molecules.

4.1 Single-photon detection

This section refers to the detection scheme (a) of Fig. 3.4, which was built by the procedure outlined in Sec. 3.5. The optical fiber with coupled fluorescence signal is inserted into a single-photon detector (SPAD), which is connected to a TDC. The number of detected counts is displayed using the time tagger software operated as counter. It is necessary to prevent any parasitic light from entering the SPAD, which is achieved by turning all the lights off, covering the whole detection part with a black cloth and adding extra black hardboard from every side, including from above.

The sample with lower dopant–host concentration was used for the measurement. For more efficient excitation of single molecules, the dichroic mirror was shifted by the micrometric screw of the linear stage into the TIRF microscopy regime. An area of the sample containing the crystal flake was found with the help of a LED source and classical camera imaging, whose gain was increased and cooling turned on. Then the setup was switched back to the laser illumination and the sample scanned around using the piezo stage until a doughnut-shaped molecule was observed in the image. Upon some of the tries, the found molecule experienced photobleaching, which was observed in the counter regime as a sudden drop in the number of counts as a function of time. The bleaching is caused by extensive exposure to the continuous laser illumination and is irreversible. Observation of this process can be considered as an indicator that only a single molecule was present. It is, however, not very useful in practice, as it only serves as a retrospective proof since the molecule becomes unable to emit any more fluorescent light afterwards.

When a stable molecule was detected, the count rate was maximized by program-controlled nano-scale translation of the piezo state, by rotation the HWP and by slightly adjusting the tip and tilt of one of the mirrors in front of the fiber collimator.

The maximum emission count rate is examined by measuring the dependence of the detected count rate on the excitation power of the laser beam. The measured dependence exhibits saturation behaviour, theoretically described by

$$C(I) = C_\infty \frac{I/I_s}{1 + I/I_s} + \alpha I, \tag{4.1}$$

which is a saturation law derived from rate equations for a two-level system [16] and the linear term is added in order to account for possible background fluorescence, which might occur especially for the high values of excitation power. C_∞ is the saturation count rate, I the excitation intensity, and I_s the saturation intensity. Both the measured data points and the curve fitted to the data according to the saturation law are shown in Fig. 4.1.

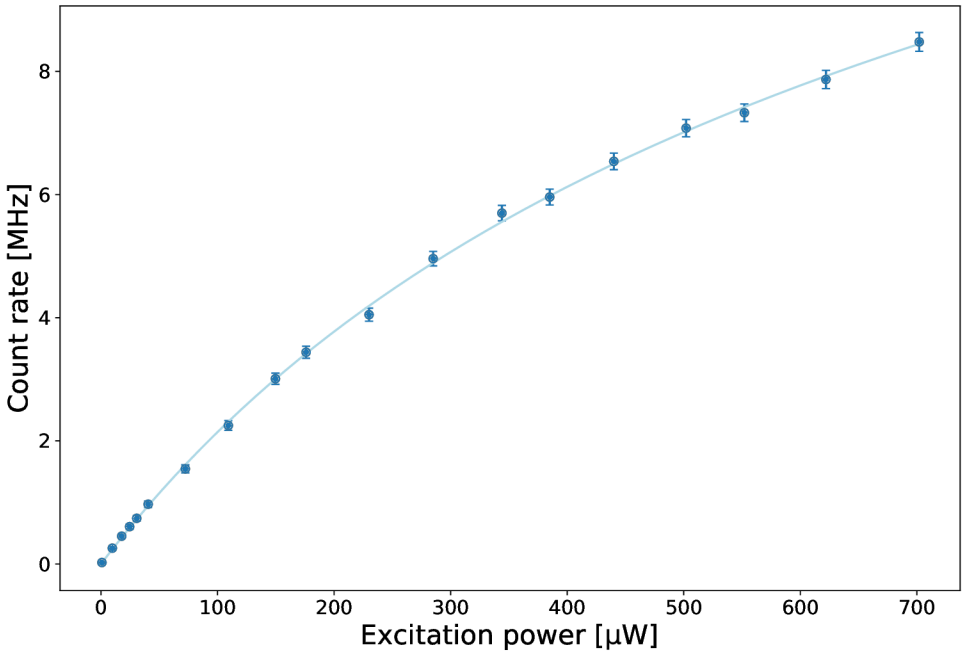

Figure 4.1: Dependence of the detected count rate on the excitation laser power showing a saturation behaviour. Fit based on Eq. (4.1) to the measured data points is depicted as the solid line.

The saturation count rate is found to be $C_\infty = 14 \pm 4$ MHz and the saturation power $I_s = 588 \pm 141\,\mu\text{W}$ from the parameters of the fit. The proportionality constant α regarding the background fluorescence is of the order of 10^{-3} and the linear term αI is therefore of the order of 10^{-1} MHz for higher values of the excitation power, which means that the background fluorescence contribution is significant. The errorbars indicate Poissonian uncertainty. The saturation intensity is typically rather high, which is due to the mutual orientation of terrylene molecules transition dipole moment and the excitation field, because only a fraction of the laser intensity is influencing the molecule [29]. Saturation of the detectors plays a minor role as it

occurs for count rates around 30 MHz. The measured count rates are nevertheless quite high and in the future it would be desirable to correct for the non-linearity of the detectors [36].

4.2 Spectrum

After data acquisition for the number of counts, the MM fiber was unplugged from the SPAD and was inserted into the spectrometer (HR2000+, Ocean Optics) instead. The spectrum of the signal emitted by a single molecule measured over integration time of 8 s is shown in Fig. 4.2.

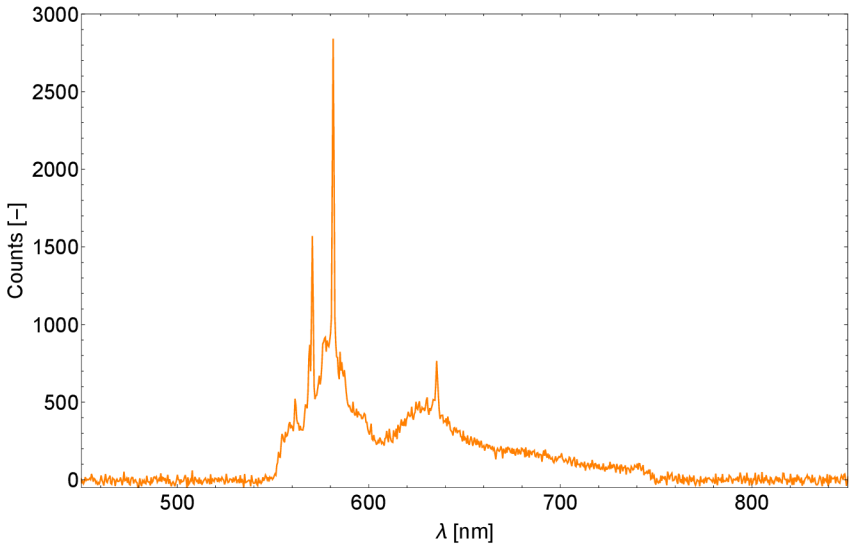

Figure 4.2: Spectrum of the fluorescence from a single terrylene molecule.

The spectrum qualitatively corresponds well to those reported in literature ([29], [37]). It is broadened due to the room-temperature conditions and two peaks corresponding to two vibronic levels are observed.

4.3 Hanbury-Brown and Twiss experiment

The ultimate goal all along was to obtain a source of single photons. In the presented experimental arrangement together with the sample of single terrylene molecules embedded in crystalline host of p-terphenyl, the single-photon sources are the single molecules. A molecule modelled by a two-level system as in Sec. 2.1 can never emit more than one photon at the same time as it ends up in the ground state after having emitted a photon and needs to be excited again before another emission can occur.

Some characteristics of the detected fluorescence light were already reported, but the most important one is still to be discussed – the experimental proof that the detected signal from a single molecule is a non-classical single-photon signal. A scheme utilized for this purpose is the Hanbury-Brown and Twiss experiment [38]. It is a correlation measurement of intensities with the use of a balanced beam

splitter and two detectors. The principle is based on the fact that coherence of a beam and the intensity fluctuations are related in the sense that the coherence time τ_c determines the fluctuations time scale [39]. The quantity to assess the intensities correlation is the second-order correlation function $g^{(2)}(\tau)$ defined as

$$g^{(2)}(\tau) = \frac{\langle I(t)I(t+\tau)\rangle}{\langle I(t)\rangle^2}, \tag{4.2}$$

for the case when the average intensity is constant, i.e. $\langle I(t)\rangle = \langle I(t+\tau)\rangle$. The brackets denote time averaging over a long period of time and τ is a time delay.

For classical light, the following applies:

$$g^{(2)}(0) \geq 1, \tag{4.3}$$

$$g^{(2)}(0) \geq g^{(2)}(\tau). \tag{4.4}$$

If the intensity $I(t)$ of a light source evolves over time, the second-order correlation function $g^{(2)}(\tau)$ will be a decreasing function of τ and will approach 1 in the limit of a large τ [39]. In case $I(t)$ is constant, which is true for a perfectly coherent light, $g^{(2)}(\tau) = 1$ at all times.

If the discrete nature of light is taken into account and the same scheme of a beam splitter and two detectors is examined on the level of single photons, a qualitatively different results are obtained. If a single photon is incident on the beam splitter, unlike classical light it cannot be divided any further and will therefore be detected only by one of the two detectors with equal probabilities. Since a single molecule is capable of emitting only one photon at a time and one photon can only be detected once, there will be no coincident detections on both detectors for a time delay $\tau = 0$. The second-order correlation function for a zero time delay will therefore be equal to zero,

$$g^{(2)}(0) = 0, \tag{4.5}$$

which can never happen for classical light (see equations (4.3) and (4.4)), it is hence a clear sign of non-classicality. Treating the electric fields as quantum-mechanical operators instead of classical waves, the second-order correlation function at zero time delay can be expressed using the photon number operator $\hat{n} = \hat{a}^\dagger\hat{a}$ in the form of

$$g^{(2)}(0) = \frac{\langle\hat{n}(\hat{n}-1)\rangle}{\langle\hat{n}\rangle^2}, \tag{4.6}$$

where the brackets denote quantum-mechanical expectation values. In the case a single photon is incident on the input of the correlation setup, the corresponding quantum state is an eigenstate of the photon number operator with an eigenvalue $n = 1$ and the Eq. (4.6) yields $g^{(2)}(0) = 0$, in agreement with Eq. (4.5). For a potential state containing two photons, $g^{(2)}(0) = 0.5$. This leads to the conclusion that if the measured value of $g^{(2)}(0) < 0.5$, it is a proof of the detected signal to be in a single-photon state.

The value of $g^{(2)}(0)$ in general classifies light as bunched ($g^{(2)}(0) > 1$), coherent ($g^{(2)}(0) = 1$) and antibunched ($g^{(2)}(0) < 1$), which is schematically indicated in Fig. 4.3. An example of a bunched light is thermal light. The probability of detecting another photon is higher at shorter times after the first detection [39]. Coherent

light is characterized by Poissonian statistics and random time intervals between successive photons. The photons of antibunched light tend to be spaced regularly and no classical analogue exists to this case. The photons emitted by a single molecule are antibunched for the reasons previously mentioned.

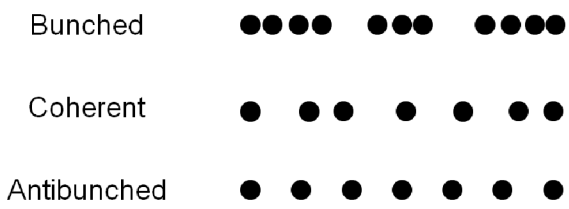

Figure 4.3: Schematic representation of a photon stream behaviour based on the second-order correlation function.

The Hanbury-Brown and Twiss (HBT) detection setup was shown in panel (b) of Fig. 3.4. The fluorescence coupled into the MM fiber is divided into two branches by a 2×2 MM fiber coupler and both outputs are connected to single-photon detectors of the same type. Both SPADs are plugged into the TDC. The time tagger software is set to counter and newly also correlation mode, which calculates the correlation function via measuring the time intervals between arrivals of photons on both detectors. The coincidence window width is 0.5 ns. The setup is shielded in the same way as in the previous section, but two filters were also added in front of the fiber collimator for in-coupling the fluorescence into the MM fiber, a long-pass filter with cut-on wavelength of 550 nm and a short-pass filter with cut-off wavelength of 750 nm so that as much of the remaining background signal as possible is eliminated. The excitation power of the laser was 33 µW throughout the measurement.

A photostable molecule was found in the sample using the same steps as before and the number of detected counts in the counter regime was optimized. When the achievable maximum was found, the measurement was switched to the correlation mode. A significant dip at the zero time delay was immediately observed. The normalized $g^{(2)}(\tau)$ curve is shown in Fig. 4.4 together with a fit to the data by a convolution

$$g^{(2)}(\tau) = \int_{-\infty}^{\infty} g^{(2)}_{\text{ideal}}(t) \cdot G(\tau - t)\, \mathrm{d}t, \tag{4.7}$$

where $g^{(2)}_{\text{ideal}}(\tau)$ is the ideal second-order correlation function for a two-level model [9] which has been assumed in the whole description of the single molecule system, and is of the form

$$g^{(2)}_{\text{ideal}}(\tau) = 1 - c \cdot \exp\left(-a\,|\tau|\right). \tag{4.8}$$

The function $G(t)$ is a Gaussian response function

$$G(t) = \frac{1}{\sqrt{2\pi}\sigma} \exp\left(\frac{-t^2}{2\sigma^2}\right), \tag{4.9}$$

which accounts for the imperfections of real detectors and electronics, namely time jitter, whose standard deviation corresponds to σ. The ideal second-order correlation function is impaired by this response function, which is expressed by the convolution.

Fig. 4.4 is the essential result of the presented work. The minimum value of the $g^{(2)}(\tau)$ fitted curve according to Eq. (4.7) for $\tau = 0$ reaches $g^{(2)}(0) = 0.25$. The standard deviation of the time jitter calculated from the parameters of the fit is equal to $\sigma = 0.60 \pm 0.03$ ns. The value comprises the jitter of both SPADs (400 ps each) and the TDC (50 ps), which yields the value of 0.57 ns, a good correspondence with the value based on the data is therefore obtained. The parameter c of the fit determines the minimal $g^{(2)}(0)$ value, which would be achieved if ideal detectors and electronics with no time jitter were used. This ideal value $g^{(2)}(0) = 0.179 \pm 0.003$. The remaining discrepancy between the minimal achievable $g^{(2)}(0)$ and 0 can be attributed to experimental imperfections such as dark counts of the SPADs and the parasitic fluorescence of the surrounding host material, whose count rate for the set excitation power is $C_{\text{host}} \sim 1$ kHz, based on the measured saturation plot shown in Fig. 4.1. Nevertheless, the measured value is considerably below the threshold of 0.5 and it is therefore confirmed that only a single molecule emitting non-classical antibunched photons was present in the experiment.

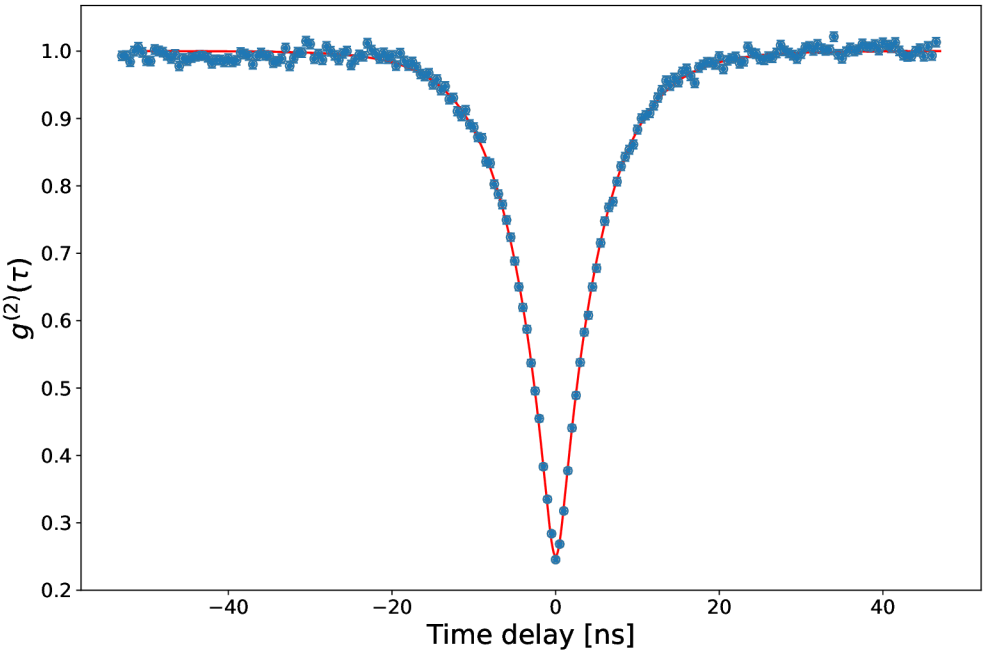

Figure 4.4: The second-order correlation function of the fluorescence signal emitted by a terrylene molecule embedded in p-terphenyl crystalline host under continuous laser illumination with the power of 33 µW measured using the HBT setup and a fit to the data (red curve). The significant dip reaches the minimum value of 0.25 for zero time delay and confirms the non-classical nature of the detected signal, which conclusively originates in a single molecule.

Chapter 5

Conclusions and outlook

The work presented in this thesis has focused on the construction of a fluorescence microscope with the aim of obtaining non-classical light emitted by a single molecule. The steps taken for this purpose include the microscope design and construction, sample preparation and fluorescence characterization.

First, general theory of single-molecule fluorescence was introduced. For practical usage of single molecules in experiments such as ours, they need to be combined with a host. Overview of the chosen terrylene molecules together with p-terphenyl as the host is followed by the sample preparation procedure involving spin coating, which is capable of creating a thin film of the solution on the glass coverslip. Detailed description of all the crucial steps of the fluorescence microscope construction is provided in Chapter 3, starting with the general design and diving into more detail by discussing individual optical components. The building process and alignment of the whole setup are covered and two different regimes of operation are mentioned.

The final chapter examines the fluorescent light emitted by terrylene molecules. The count rate was measured in dependence on the excitation laser power and saturation behaviour was observed. The saturation count rate and saturation intensity for the particular molecule were concluded to be $C_\infty = 14 \pm 4$ MHz and $I_s = 588 \pm 141\,\mu\text{W}$ from the fitting curve. Spectrum of the single-molecule fluorescence was also shown. The crucial result of the thesis is the second-order correlation function $g^{(2)}(\tau)$ measured by the means of Hanbury-Brown and Twiss experiment. Its minimum value at a zero time delay τ is found to be $g^{(2)}(0) = 0.25$. The standard deviation of the used detectors and electronics time jitter determined from the fitted curve is $\sigma = 0.60 \pm 0.03$ ns. If the SPADs and TDC were ideal and had no time jitter, the minimum achievable second-order correlation function value would be $g^{(2)}(0) = 0.179 \pm 0.003$. Both the measured convolved and the minimum achievable value of $g^{(2)}(0)$ clearly suggest that the fluorescent light present in the experiment exhibits antibunching behaviour. This finding provides an evidence for the single-photon nature of the emitted fluorescence and supports the suitability of the terrylene in p-terphenyl system as a single-photon source for applications in quantum optics and quantum information processing.

The fluorescence microscope for single-photon emitter imaging is rather a recent project of the Quantum Optics Lab Olomouc (QOLO). The experimental setup presented in this thesis was the first iteration, which led to successful demonstration that the microscope is capable of fluorescence imaging and of achieving non-classical

single-photon signal, as evidenced by the measured $g^{(2)}(\tau)$ function. There were, however, several drawbacks to it, which we are now aiming to overcome with a new, rebuilt setup with a slightly different layout in order to make a better use of the available space. The first shortcoming to mention that was fixed while building the new setup is a control of the excitation laser power at the input of the experiment. Since the laser light was outcoupled directly into the setup at first, it was only possible to regulate the power by the ND filters with different optical densities or directly in the control software of the laser, which the manufacturers do not generally recommend as the laser should be running at a constant power for some time to ensure optimal operation. Therefore, in the new setup, a power-control block based on a combination of HWP, QWP and a linear polarizer was added before the beam enters the microscope setup, which allows for a continuous and precise adjustment of the laser power. Moreover, the standard mirror placed at 45° angle under the microscope stage and reflecting light up into the objective was substituted with a mirror of the same properties, but with 1.5 inch diameter to assure that no signal both from the excitation and fluorescence is lost. The 45° mount was also replaced with a custom robust mount from stainless steel.

In the future, further possible enhancements lie in employing a pulsed laser rather than the continuous one for the single-photon source to be deterministic, which cannot be achieved under a continuous illumination. Furthermore, it would be interesting to investigate the behaviour of other fluorescent molecules in various host materials and under different conditions. A diamond crystal containing nitrogen-vacancy centres has already been acquired, as well as anthracene as an alternative host material for terrylene molecules.

The current goal is to improve the second-order correlation function and bring the value of $g^{(2)}(0)$ even closer to zero, as well as perform more complex analysis and detection schemes on the fluorescence signal in order to study its photon statistics. The statistical and correlation measurements can yield information useful for utilizing the molecules as sensors, which is challenging at room temperatures and therefore provides room for novel research potentially leading to wide range of applications which are now limited to cryogenic temperatures.

Last but not least, the limits of imaging resolution can be pushed further and the molecules could also serve as point sources for optical systems testing, as the single molecules are as close to an ideal point source as practice allows.

Bibliography

[1] B. Y. Zel'dovich and D. N. Klyshko, "Field statistics in parametric luminescence," *Jetp Letters*, vol. 9, p. 40, 1969.

[2] A. I. Lvovsky, H. Hansen, T. Aichele, O. Benson, J. Mlynek, and S. Schiller, "Quantum state reconstruction of the single-photon Fock state," *Physical Review Letters*, vol. 87, p. 050402, 2001.

[3] S. Kück, M. López, H. Hofer, H. Georgieva, J. Christinck, B. Rodiek, G. Porrovecchio, M. Šmid, S. Götzinger, C. Becher, P. Fuchs, P. Lombardi, C. Toninelli, M. Trapuzzano, M. Colautti, G. Margheri, I. P. Degiovanni, P. Traina, S. Rodt, and S. Reitzenstein, "Single photon sources for quantum radiometry: a brief review about the current state-of-the-art," *Applied Physics B*, vol. 128, p. 28, 2022.

[4] J. McKeever, A. Boca, A. D. Boozer, R. Miller, J. R. Buck, A. Kuzmich, and H. J. Kimble, "Deterministic generation of single photons from one atom trapped in a cavity," *Science*, vol. 303, pp. 1992–1994, 2004.

[5] M. Hennrich, T. Legero, A. Kuhn, and G. Rempe, "Photon statistics of a non-stationary periodically driven single-photon source," *New Journal of Physics*, vol. 6, pp. 86–86, 2004.

[6] C. Maurer, C. Becher, C. Russo, J. Eschner, and R. Blatt, "A single-photon source based on a single Ca^+ ion," *New Journal of Physics*, vol. 6, pp. 94–94, 2004.

[7] R. Alléaume, F. Treussart, G. Messin, Y. Dumeige, J.-F. Roch, A. Beveratos, R. Brouri-Tualle, J.-P. Poizat, and P. Grangier, "Experimental open-air quantum key distribution with a single-photon source," *New Journal of Physics*, vol. 6, pp. 92–92, 2004.

[8] T. M. Babinec, B. J. M. Hausmann, M. Khan, Y. Zhang, J. R. Maze, P. R. Hemmer, and M. Lončar, "A diamond nanowire single-photon source," *Nature Nanotechnology*, vol. 5, pp. 195–199, 2010.

[9] N. Mizuochi, T. Makino, H. Kato, D. Takeuchi, M. Ogura, H. Okushi, M. Nothaft, P. Neumann, A. Gali, F. Jelezko, J. Wrachtrup, and S. Yamasaki, "Electrically driven single-photon source at room temperature in diamond," *Nature Photonics*, vol. 6, pp. 299–303, 2012.

[10] S. Kako, C. Santori, K. Hoshino, S. Götzinger, Y. Yamamoto, and Y. Arakawa, "A gallium nitride single-photon source operating at 200 K," *Nature Materials*, vol. 5, pp. 887–892, 2006.

[11] S. Strauf, N. G. Stoltz, M. T. Rakher, L. A. Coldren, P. M. Petroff, and D. Bouwmeester, "High-frequency single-photon source with polarization control," *Nature Photonics*, vol. 1, pp. 704–708, 2007.

[12] M. Bozzio, M. Vyvlecka, M. Cosacchi, C. Nawrath, T. Seidelmann, J. C. Loredo, S. L. Portalupi, V. M. Axt, P. Michler, and P. Walther, "Enhancing quantum cryptography with quantum dot single-photon sources," *npj Quantum Information*, vol. 8, p. 104, 2022.

[13] Y. Arakawa and M. J. Holmes, "Progress in quantum-dot single photon sources for quantum information technologies: A broad spectrum overview," *Applied Physics Reviews*, vol. 7, p. 021309, 2020.

[14] T. Basché, W. E. Moerner, M. Orrit, and H. Talon, "Photon antibunching in the fluorescence of a single dye molecule trapped in a solid," *Physical Review Letters*, vol. 69, pp. 1516–1519, 1992.

[15] S. C. Kitson, P. Jonsson, J. G. Rarity, and P. R. Tapster, "Intensity fluctuation spectroscopy of small numbers of dye molecules in a microcavity," *Physical Review A*, vol. 58, pp. 620–627, 1998.

[16] B. Lounis and W. E. Moerner, "Single photons on demand from a single molecule at room temperature," *Nature*, vol. 407, pp. 491–493, 2000.

[17] W. E. Moerner, "Single-photon sources based on single molecules in solids," *New Journal of Physics*, vol. 6, pp. 88–88, 2004.

[18] X.-L. Chu, S. Götzinger, and V. Sandoghdar, "A single molecule as a high-fidelity photon gun for producing intensity-squeezed light," *Nature Photonics*, vol. 11, pp. 58–62, 2016.

[19] A. Fasoulakis, K. D. Major, R. A. Hoggarth, P. Burdekin, D. P. Bogusz, R. C. Schofield, and A. S. Clark, "Uniaxial strain tuning of organic molecule single photon sources," *Nanoscale*, vol. 15, pp. 177–184, 2023.

[20] S. Lukishova, A. Schmid, A. McNamara, R. Boyd, and C. Stroud, "Room temperature single-photon source: single-dye molecule fluorescence in liquid crystal host," *IEEE Journal of Selected Topics in Quantum Electronics*, vol. 9, pp. 1512–1518, 2003.

[21] C. Degen, F. Reinhard, and P. Cappellaro, "Quantum sensing," *Reviews of Modern Physics*, vol. 89, p. 035002, 2017.

[22] M. A. Taylor and W. P. Bowen, "Quantum metrology and its application in biology," *Physics Reports*, vol. 615, pp. 1–59, 2016.

[23] M. Lelek, M. T. Gyparaki, G. Beliu, F. Schueder, J. Griffié, S. Manley, R. Jungmann, M. Sauer, M. Lakadamyali, and C. Zimmer, "Single-molecule localization microscopy," *Nature Reviews Methods Primers*, vol. 1, p. 39, 2021.

[24] R. W. Taylor and V. Sandoghdar, "Interferometric scattering (iSCAT) microscopy and related techniques," in *Biological and Medical Physics, Biomedical Engineering*, pp. 25–65, Springer International Publishing, 2019.

[25] M. Dahmardeh, H. M. Dastjerdi, H. Mazal, H. Köstler, and V. Sandoghdar, "Self-supervised machine learning pushes the sensitivity limit in label-free detection of single proteins below 10 kDa," *Nature Methods*, vol. 20, pp. 442–447, 2023.

[26] O. Schwartz, J. M. Levitt, R. Tenne, S. Itzhakov, Z. Deutsch, and D. Oron, "Superresolution microscopy with quantum emitters," *Nano Letters*, vol. 13, pp. 5832–5836, 2013.

[27] M. Fox, *Optical Properties of Solids*. Oxford University Press, 2010.

[28] J. L. Skinner and W. E. Moerner, "Structure and dynamics in solids as probed by optical spectroscopy," *The Journal of Physical Chemistry*, vol. 100, pp. 13251–13262, 1996.

[29] F. Kulzer, F. Koberling, T. Christ, A. Mews, and T. Basché, "Terrylene in p-terphenyl: single-molecule experiments at room temperature," *Chemical Physics*, vol. 247, pp. 23–34, 1999.

[30] S. Kummer, T. Basché, and C. Bräuchle, "Terrylene in p-terphenyl: a novel single crystalline system for single molecule spectroscopy at low temperatures," *Chemical Physics Letters*, vol. 229, pp. 309–316, 1994.

[31] S. Kummer, F. Kulzer, R. Kettner, T. Basché, C. Tietz, C. Glowatz, and C. Kryschi, "Absorption, excitation, and emission spectroscopy of terrylene in p-terphenyl: Bulk measurements and single molecule studies," *The Journal of Chemical Physics*, vol. 107, pp. 7673–7684, 1997.

[32] R. M. Dickson, D. J. Norris, and W. E. Moerner, "Simultaneous imaging of individual molecules aligned both parallel and perpendicular to the optic axis," *Physical Review Letters*, vol. 81, pp. 5322–5325, 1998.

[33] R. Pfab, J. Zimmermann, C. Hettich, I. Gerhardt, A. Renn, and V. Sandoghdar, "Aligned terrylene molecules in a spin-coated ultrathin crystalline film of p-terphenyl," *Chemical Physics Letters*, vol. 387, pp. 490–495, 2004.

[34] E. ten Grotenhuis, J. van Miltenburg, and J. van der Eerden, "Preparation of anthracene micro-crystals by spin-coating and atomic force microscopy study of the molecular packing," *Chemical Physics Letters*, vol. 261, pp. 558–562, 1996.

[35] K. N. Fish, "Total internal reflection fluorescence (TIRF) microscopy," *Current Protocols in Cytometry*, vol. 50, p. 12, 2009.

[36] J. Hloušek, I. Straka, and M. Ježek, "Experimental observation of anomalous supralinear response of single-photon detectors," *Applied Physics Reviews*, vol. 10, p. 011412, 2023.

[37] S.-J. Yoon, C. T. Trinh, and K.-G. Lee, "Coherence studies of photons emitted from a single terrylene molecule using michelson and young's interferometers," *Journal of the Optical Society of Korea*, vol. 19, pp. 555–559, 2015.

[38] R. H. Brown and R. Q. Twiss, "Correlation between photons in two coherent beams of light," *Nature*, vol. 177, pp. 27–29, 1956.

[39] M. Fox, *Quantum Optics: An Introduction*. Oxford University Press, 2006.